High-Intensity Laser Interactions with Mass-Limited Solid Targets and Implications for Fast-Ignition Experiments on OMEGA EP

Introduction

Picosecond laser–solid interaction at relativistic intensities has generated a high level of experimental[1–5] and theoretical[6–9] interest in recent years. This is due to its relevance to the fast-ignitior (FI) scheme for achieving inertial confinement fusion (ICF)[10,11] and to backlighter development for the x-ray radiography of dense materials.[12,13]

The interaction of high-intensity, $I \sim (10^{18}$ to $10^{21})$ W/cm^2, picosecond laser pulses with solid targets produces copious energetic electrons. Remarkable conversion efficiencies of up to 40% of the incident laser energy have been reported,[1,14] with characteristic electron energies ranging from ~100 keV up to several MeV.[14–16]

When these energetic electrons propagate into the bulk of a solid target, hard-x-ray bremsstrahlung and characteristic inner-shell line emission are produced [the first observations of K_α radiation from picosecond laser–produced plasmas were presented as early as 1979 (Ref. 17)]. The brightness of this radiation, either continuous or line emission, makes it valuable for x-ray radiography of ICF implosions, a primary motivation for the recent experiments of Theobald *et al.*, reported in Ref. 18. This article investigates, using semi-analytic and implicit-hybrid particle-in-cell (PIC) modeling,[19,20] the K-shell line emission from mass-limited targets and compares the predictions with these experiments.

The inner-shell line emission provides information on the energetic electrons produced in the interaction and its subsequent transport and heating of the target.[1,4,21–37] The main conclusion is that mass-limited targets of mid-Z elements provide an excellent "test bed" for FI physics due to simplifications afforded by the near-perfect hot-electron refluxing and by the effects on the line emission caused by the target heating.

Electron "refluxing" within the target, due to reflection from the surface sheath fields, is well known[9,28,29] and is connected to the generation of fast protons and ions.[30,31] When considering the generation of secondary radiation, this effect has not always been taken into account, e.g., Refs. 32–34. Unlike the case of proton acceleration,[9,28] the effect of hot electrons refluxing on the K-shell production efficiency has not been described, rather the emphasis has been placed on the energy dependence of the K-shell ionization cross section[34] and the competition with penetration depth and reabsorption of the characteristic radiation,[26,35] which is appropriate for massive targets.

It is shown here that the K-shell yields, per joule of hot electrons, of mass-limited targets are insensitive to the hot-electron spectrum and laser intensity. This is valid as long as the hot-electron stopping is classical and arises because of the energy dependence of the K-shell ionization cross section and electron range. It requires that relativistic corrections to the K-shell ionization cross section are accounted for.[36] The intensity dependence of K-shell production efficiency, expressed per joule of incident laser energy, is sensitive to the hot-electron conversion efficiency $\eta_{L\to e}(I)$. The experimental K_α yields from Ref. 18 are found to be consistent with the model if an intensity-independent hot-electron conversion efficiency of $\eta_{L\to e} = 10\%$ is assumed over the range $10^{18} < I < 10^{20}$ W/cm^2.

Volumetric heating of reduced-mass targets[18] is predicted to be sufficient that ionization of the copper M shell will strongly affect the ratio of K_β to K_α emission.[21] Three-dimensional *LSP* calculations,[19,20] including the relevant atomic processes,[27] have been performed for parameters of the RAL (Rutherford Appleton Laboratory) experiments and spatially resolved images of both K_α and K_β emission have been produced. It is shown that these measurements can be used to infer the degree of bulk heating and provide a *consistency check* on the hot-electron conversion efficiency obtained by fitting the absolute K_α-photon yields. A comparison between the predicted ratio of K_β- to K_α-photon production, for $\eta_{L\to e} = 10\%$, with the experimentally observed ratios is not conclusive. Rather, it suggests the usefulness of the technique, which will be pursued in future experiments on OMEGA EP currently under construction at LLE.[38]

The following sections (1) summarize the Theobald *et al.*[18] experiments, (2) describe a semi-analytic model for K-shell line emission in mass-limited targets, (3) compare the modeling pre-

dictions with the RAL experiments, (4) present the *LSP* calculations of volumetric heating, and (5) present the conclusions.

RAL PW and 100-TW Experiments

Pulses of 1.06-μm laser light from either the RAL Petawatt (PW) or the 100-TW Facility were focused with an *f*/3 off-axis parabola to ~10- to 100-μm spots onto Cu foil targets, achieving laser intensities between 3×10^{18} to 4×10^{20} W/cm^2. The foil thicknesses ranged between $d = 1$ to 75 μm, and the areas from $A = 0.01$ to 8.0 mm^2, resulting in target volumes of $V = 10^{-5}$ to 10^{-1} mm^3. The pulse durations ranged from 0.4 to 10 ps. Inner-shell emission and resonance-line emission occurred in these experiments. The K_α and K_β lines are emitted by the inner-shell transitions when an L- or M-shell electron fills a vacancy in the K shell, respectively, and the corresponding excess energy is radiated away by a photon in competition with Auger decay. Both x rays and energetic electrons may produce K-shell vacancies, assuming that the radiation has sufficient energy to excite above the K edge (for Cu, $h\nu > 9$ keV). Indirect inner-shell emission due to absorption of continuous x-ray radiation that is produced while suprathermal electrons decelerate in the target is negligible for elements with an atomic number $Z < 30$ (Refs. 37 and 39). Energetic electrons are the main contribution to K_α and K_β production in high-intensity, ultrashort, laser–solid interaction with low- and mid-*Z* materials.[24,26] X-ray spectra were collected, and the total number of K_α and K_β photons emitted, per unit laser energy, were obtained as described in Theobald *et al.*[18] The resonance-line emission is not discussed here.

In contrast with previous experiments using massive targets, absorption of the characteristic x rays is modest. As a result, the mechanism controlling the intensity dependence of the K_α yield is no longer the interplay between the electron penetration depth relative to the K-photon attenuation length as in earlier experiments.[26,40] A different model is required to predict the K-shell yield and its dependence on interaction parameters.

Description of a Semi-Analytic Model

The absolute K-shell photon yield N_k is the sum of the yield from two hot-electron populations: (1) electrons that escape from the target after losing only part of their energy (l), and (2) electrons that reflux, losing all of their energy to the target (r), i.e., $N_k = (N_k)_l + (N_k)_r$. The distinction is of significance only for targets thinner than the expected electron range in the material. For copper, this corresponds to targets thinner than a few millimeters for interaction intensities of ~10^{19} W/cm^2.

A simple estimate of the "refluxing efficiency," which is the ratio of the number of electrons stopped in the target to the total, $\eta_r = \left(N_e - N_l\right)/N_e$, can be given roughly by estimating the capacitance of the target. Assuming the target is a perfectly conducting thin disk in vacuum, $C = 8\,\epsilon_0 r \sim 70.8 \times 10^{-12}\,r$ farads, where r is the radius of the disk in meters, then a loss of $N_l = 4.42 \times 10^{11}$ (r/1 mm) (V/1 MV) electrons is required to produce a potential drop V in a target of radius r. This will be modified if the target is not isolated, for example, by a conducting target stalk. The required potential is determined self-consistently so that, for Boltzmann-distributed electrons at a temperature T, the potential satisfies $N_l = N_e \exp(-\mathrm{eV}/T)$. This leads to the equation $\exp(-\Phi) = \kappa\Phi$, where $\Phi = \mathrm{eV}/T$ and κ is given by $\kappa = 7.08 \times 10^{-2} rT^2/\left(\eta_{L\to e}\,E_L\right)$, where r is in mm, T is in MeV, and E_L is in joules. This can be solved for Φ, giving the refluxing efficiency $\eta_r = 1 - \exp(-\Phi)$, with the results for varying laser intensity and foil radius shown in Fig. 109.36. Note that the efficiency is extremely high for the parameters of the RAL experiments, $\eta_r > 90\%$.

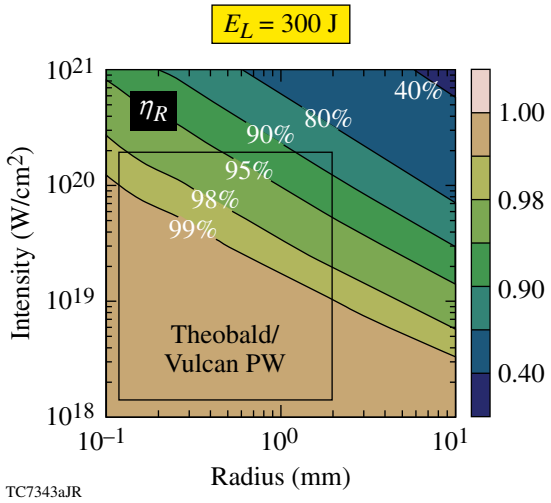

Figure 109.36
Refluxing efficiency obtained from the capacitance model. The hot-electron temperature is assumed to depend on laser intensity according to the ponderomotive scaling.[6]

The refluxing electrons are prevented from escaping by the self-consistent electromagnetic fields, so that the electron stopping can be treated as if the electrons were propagating in an infinite medium. The K-photon yield $(N_k)_r$ is computed by integrating along the path of electrons whose initial energies are described by an energy distribution $f(E_0)$ as long as (1) energy loss is accurately described with a continuous slowing-down formula ($\mathrm{d}E/\mathrm{d}s$), and (2) cold cross sections $\sigma_K(E)$ for K-shell ionization are appropriate (note that for copper $Z = 29$, only direct K-shell ionization is significant[37]). The contribution to the total yield N_k due to refluxing electrons $(N_k)_r$ is then given by

$$\left(N_k\right)_r = \left(\eta_r N_e\right)\int_0^\infty \mathrm{d}E_0 f\left(E_0\right)\int_{E_0}^0 \mathrm{d}E\omega_k n_{\mathrm{Cu}}\sigma_k\left(\frac{\mathrm{d}E}{\mathrm{d}s}\right)^{-1} \quad (1)$$

$$= \left(\eta_r N_e\right) n_{\mathrm{Cu}}\omega_k\int_0^\infty \mathrm{d}E_0 f\int_0^{s\left(E_0\right)} \mathrm{d}s\sigma_k\left[E\left(E_0,s\right)\right], \quad (2)$$

where N_e is the total number of hot electrons, ω_k is the fluorescence yield ($\omega_k = 0.44$ for Cu)[41] (the fraction of K-ionization events resulting in K-quantum emission), and n_{Cu} is the number density of copper atoms in the target. The contribution from the "loss" electrons $(N_k)_l$ is similarly obtained to the above but by replacing η_r with $1–\eta_r$ and truncating the electron path length s in the integral Eq. (2) whenever it exceeds the target thickness $s\left(E_0\right) \rightarrow s_{\max} = \min\left[s\left(E_0\right), d\right]$ (if the target is thick enough so that multiple scattering is important, an accurate calculation of this term would require a Monte Carlo calculation). To distinguish between the K-emission lines, e.g., K_β, $K_{\alpha 1}$, $K_{\alpha 2}$, etc., of corresponding energies $\epsilon_{K_i} = 8.906$, 8.048, and 8.028 keV, respectively, the relative emission probabilities p_i are introduced, defined according to $N_{K_i} = p_i N_k$, where "i" stands for either "β," "α_1," or "α_2." The probabilities are taken to be $p_a\left(= \Sigma_{i=\alpha_1,\alpha_2} p_i\right)$, $p_\beta = 0.88$, 0.12, respectively, whose values correspond to cold Cu at solid density.[42] From this model the electron-to-K-photon generation efficiency $\eta_{e\rightarrow k}$ is determined. This is defined as $E_k = \eta_{e\rightarrow k} E_e$, where the energy in electrons is given by $E_e = N_e\langle E_e\rangle$, and in K photons by $E_k = \epsilon_k N_k$. Here ϵ_k is the average fluorescence energy $\epsilon_K = \sum_i p_i\epsilon_{K_i}$ (8.14 keV for copper) and $\left\langle E_e\right\rangle = \int \mathrm{d}EEf(E)$ is the average electron energy, resulting in

$$\eta_{e\rightarrow k} = n_{\mathrm{Cu}}\omega_k\frac{\epsilon_k}{\left\langle E_e\right\rangle}$$

$$\times\left\{\eta_r\int_0^\infty \mathrm{d}E_0 f\left(E_0\right)\int_0^{s\left(E_0\right)} \mathrm{d}s\sigma_k\left[E\left(E_0,s\right)\right]\right.$$

$$\left.+\left(1-\eta_r\right)\int_0^\infty \mathrm{d}E_0 f\int_0^{s_{\max}} \mathrm{d}s\sigma_k\left[E\left(E_0,s\right)\right]\right\}. \quad (3)$$

A direct comparison between the experimental production efficiency (yield/laser joule) and the calculated generation efficiency is not straightforward. The experimentally observable quantity $N_{k,\mathrm{obs}}$ requires a knowledge of the detector solid angle, the filter, and detector efficiency.[18] Given this, the efficiency

$$\eta_{e\rightarrow k} = \frac{\epsilon_k\left(N_{k,\mathrm{obs}}/f_{\mathrm{abs}}\right)}{\eta_{L\rightarrow e}E_L} \quad (4)$$

may be computed only if the K-shell photon reabsorption fraction f_{abs} and the hot-electron production efficiency $\eta_{L\rightarrow e} = E_e/E_L$ are known. E_L is the energy in the laser pulse. The absorption fraction f_{abs} can be easily computed,[43] but the electron-production efficiency is subject to a great deal of uncertainty.[1] In principle, this could depend on many factors, $\eta_{L\rightarrow e} = \eta_{L\rightarrow e}(I_L, E_L, \nabla\log n, \ldots)$, where, for example, I_L is the laser intensity, E_L is the laser energy, and $\nabla\log n_e$ is the electron-plasma density scale length.[31,44] For current purposes it is either treated as a free "fitting" parameter, or taken to be a function of laser intensity only, with the dependence as given by Ref. 27, a fit to data obtained on the Nova Petawatt.[1] The predicted efficiency, obtained using Eq. (3), requires further specification of the hot-electron spectrum $f(E)$. Exponentially distributed electron energies are assumed, $f(E)\mathrm{d}E = (1/T)\exp(–E/T)\mathrm{d}E$, and the laser intensity connected to the temperature T, equal to the average energy for an exponential distribution, $\langle E\rangle = T$, using the "ponderomotive scaling" of Wilks,[6,45] $T = 0.511\left[\left(1 + I_{18}\lambda_{\mu\mathrm{m}}^2/1.37\right)^{1/2} - 1\right]$ MeV. Different intensity-temperature scalings have been proposed in the literature.[46,47] The calculations have also been performed with a relativistic Maxwellian (Jüttner) distribution,[48] leading to no change in the overall conclusions.

Equation (3), using ITS (Integrated Tiger Series) data for hot-electron stopping power and K-shell ionization cross sections,[49,50] the fluorescence probability, and the relative emission probabilities, taken together with the absorption fraction, the refluxing fraction, the hot-electron conversion efficiency, the hot-electron distribution function, and hot-electron temperature scaling as described in the text fully defines the model. From this the conversion efficiency of laser energy to K photons $\eta_{L\rightarrow k}$ can be computed with no free parameters.

Comparison Between the Modeling and RAL Experimental Results

Figure 109.37 shows K_α-photon yield, per joule of laser energy, as a function of laser intensity from the model described above with constant hot-electron conversion efficiencies of $\eta_{L\rightarrow e} = 10\%$ and 20% (solid curves). The predicted K_α production efficiency is almost independent of laser intensity over the range $I = 2\times 10^{18}$ to 2×10^{20} W/cm^2 and takes the value $(\eta_{L\rightarrow k})_{\mathrm{model}} \sim 4\times 10^{-4}$ for $\eta_{L\rightarrow e} = 10\%$. This is consistent with experimental data taken from shots with 200 to 500 J of laser energy on a 20-μm-thick target (black triangles). Although not the case in Fig. 109.38, the experimental data are usually corrected for absorption and not the model predictions. The independence of efficiency on hot-electron temperature (laser intensity) over the experimental range of intensities can

be understood if perfect refluxing is assumed: the number of K-shell photons per electron is essentially given by the product of the range $s_0 \equiv s(E_0) = \int_{E_0}^{0} dE(dE/ds)^{-1}$ and the probability

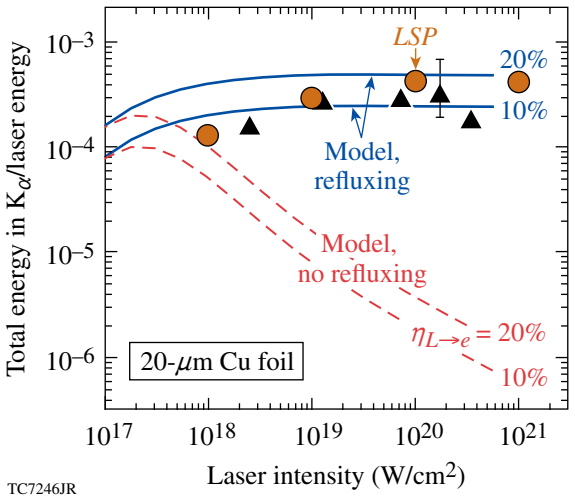

Figure 109.37
K_α production efficiency versus laser intensity for 20-μm-thick foils. The semi-analytic model with refluxing and a 10% hot-electron conversion efficiency (lower solid line) agrees with the *LSP* calculation (circles) and the experimental data (triangles). Also shown are the model predictions with no refluxing (dashed lines). The predictions, and not the data, have been corrected for reabsorption in the target.

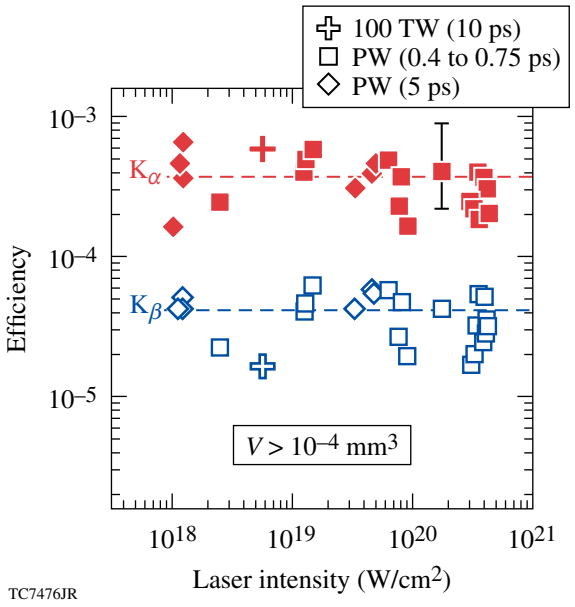

Figure 109.38
Experimental K_α (solid markers) and K_β (open markers) production efficiency as a function of laser intensity for both the 100-TW laser system (crosses) and the PW laser for short pulses (squares) and long pulses (diamonds). Only targets having a volume greater than 10^{-4} mm^3 are shown.

of K-shell emission per unit path $\omega_k n_{Cu} \sigma_k(E_0)$ [Eq. (1)]. When normalized by E_0, this product is a very weak function of the electron energy, provided that the relativistic corrections to the cross section $\sigma_k(E)$ are properly taken into account.[51] If the refluxing is ignored, $\eta_r \to 0$, then the dashed curves result. The *LSP* predictions, shown as circles in Fig. 109.37, are very similar to the semi-analytic model. This is to be expected because *LSP* uses the same cross sections as the model and the stopping is found to be due to classical collisions and not anomalous mechanisms. The discrepancies are a result of the approximations in the *LSP* collision model.[20]

Agreement can be obtained only for high refluxing efficiency, $\eta_r \sim 100\%$, leading to the broad conclusion that reduced-mass targets produce the same number of K photons as targets of infinite thickness (but without the reabsorption). It follows that the K-shell yield is independent of the target geometry (volume). As Fig. 109.38 shows, this is actually observed.

Figure 109.38 shows both the K_α- (solid markers) and K_β-photon production efficiencies (open markers) from both the 100-TW system (crosses) and the RAL PW (squares and diamonds) as a function of laser intensity for a range of target geometries having volumes $10^{-4} < V < 10^{0}$ mm^3. (The target thicknesses employed were 20 μm for the 100-TW shots, 5 to 75 μm for the PW shots with 5-ps pulses, and 5 to 25 μm for the PW shots with 0.4- to 0.75-ps pulses.) The yields are essentially constant and the ratio of K_β/K_α is consistent with the expected cold matter value $N_{K_\beta}/N_{K_\alpha} = 0.14$. The predictions of the semi-analytic model with $\eta_{L\to e} = 10\%$ are shown as dashed lines.

A hot-electron conversion efficiency of 10% is lower than the $\eta_{L\to e} \sim (20\%–40\%)$ quoted in the literature for these intensities, e.g., in Ref. 15. Reference 1 suggests that the conversion efficiency $\eta_{L\to e}$ rises significantly with laser intensity with efficiencies of $\eta_{L\to e} \sim 40\%$ for laser intensities of 10^{20} W/cm^2. Figure 109.39 shows the predicted K_α yield from the model as a function of laser intensity when the functional form of $\eta_{L\to e}$ is fit to the Nova PW data.[1,27] The solid lines are lines of constant conversion efficiency $\eta_{L\to e}$ and the shaded area, bounded by the dashed curves, is the prediction of the model with a reasonable allowance made for scatter in the data of Ref. 1. With the conversion efficiency prescribed in this way, there are no free parameters in the model.

The discrepancy between the simple model and the experiment at high, $I \gtrsim 1 \times 10^{19}$ W/cm^2, and low, $I \sim 10^{18}$ W/cm^2, intensities might have several causes. Additional energy-loss

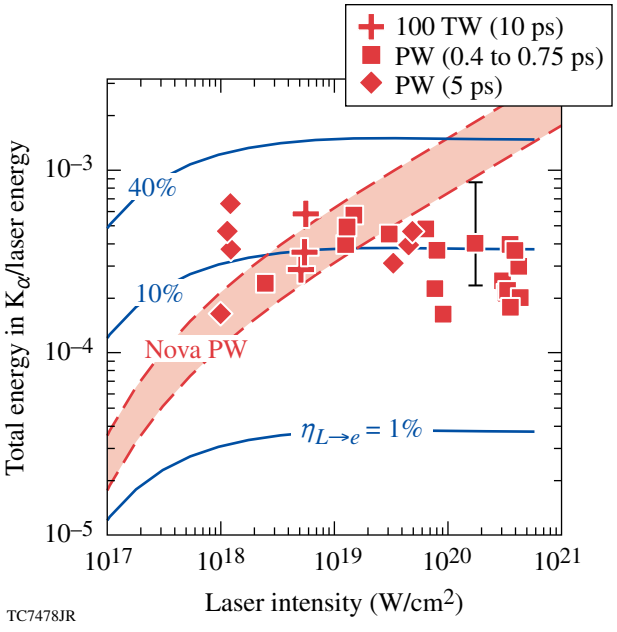

Figure 109.39
Experimental K_α production efficiency from the 100-TW system (crosses) and PW laser system with short pulses (squares) and long pulses (diamonds) as a function of laser intensity. The predictions of the semi-analytic model with hot-electron conversion efficiencies taken from a fit to Nova PW data are indicated by the shaded area bounded by dashed lines. The solid curves are lines of constant hot-electron conversion efficiency.

channels for the hot electrons such as the acceleration of protons (or ions) from the back side of the target, "anomalous" stopping mechanisms such as resistive inhibition,[52] or current filamentation instabilities, presumably becoming more important at higher intensities[9] are potential candidates. Large magnetic fields could bottle energy up at the surface,[53] where the plasma is too hot to produce K photons.

An experimentally verifiable consistency check on the inferred hot-electron conversion efficiencies, computed by fitting the absolute K_α yields, can be made by considering the volumetric heating created by the hot electrons. The collisional dissipation of the fast electrons, or the return current of the slower electrons, will volumetrically heat the foil on the picosecond time scale. The heating on this time scale, the same time scale as the K-shell emission, can be due only to the hot electrons and will be a measure of their energy content. The target heating can be quantified by measuring the ratio of K_β to K_α emission N_{K_β}/N_{K_α} because for the expected temperature rise $T \gtrsim 100$ eV, significant ionization of the M shell is expected[21] (Fig. 109.40). Smaller-mass targets are expected to achieve higher temperatures since an equal amount of energy is deposited in a smaller volume.[21]

Figure 109.40 shows the ionization degree Z^* for solid-density copper as a function of temperature according to the Thomas–Fermi model.[54] The main part of the figure shows an estimate of the line ratio as a function of temperature based on this ionization (the cold ratio has been weighted by the relative population of the M shell). It is not straightforward to estimate the ratio of the absolute K_α and K_β yields because the heating rate is a function of time and space, as is the hot-electron population. To take this properly into account we have performed *LSP* calculations.

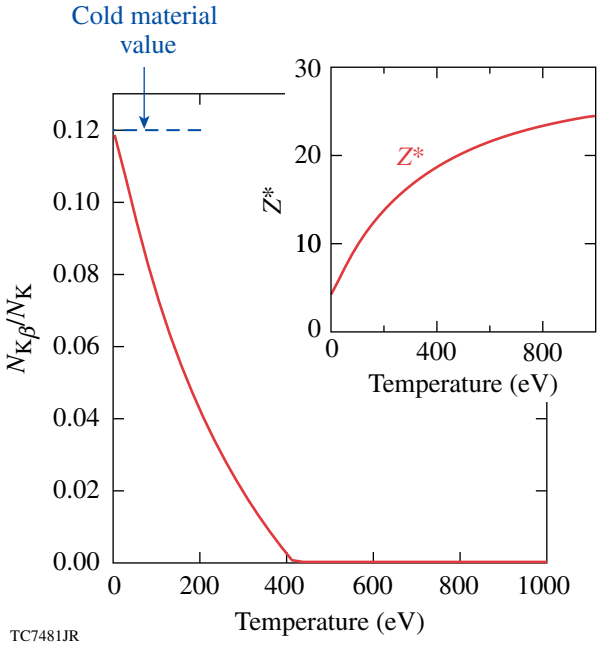

Figure 109.40
Reduction in the ratio of K_β to total K-emission probability as a function of plasma temperature, based on the Thomas–Fermi average ionization state Z^* (inset).

LSP Calculations of Volumetric Target Heating

Three-dimensional numerical calculations of target heating and K-shell emission were performed using *LSP*.[19,20] The targets were square copper foils of either (80×80) μm^2 or (160×160) μm^2 area, and either 10 μm or 20 μm in thickness. The hot-electron source was prescribed, as is usual in MC and implicit-hybrid calculations.[26,53] Electrons from the cold bulk were promoted in energy inside a region defined laterally by the laser spot and extending to a depth of 0.5 μm into the target. The rate of promotion was defined so that the power translated into the electrons was a constant fraction $\eta_{L\to e}$ of the assumed incident laser power. The energy spectrum of the promoted electrons was an isotropic Maxwellian with an average energy defined according to the local laser intensity on the surface of

the foil (assuming the ponderomotive scaling). A realistic laser spot shape was assumed, taken from Ref. 55, where 50% of the energy is contained within a characteristic diameter, $a_0 \sim 16\ \mu$m. A radial temperature dependence of the hot electrons resulted from the assumed axial symmetry of the spot, similar to that of Ref. 26. The total injected hot-electron kinetic energy was taken to be either 10 or 30 J, with a pulse duration of 0.5 or 1.5 ps, respectively. This held the average laser intensity over the central spot constant at $I = 1.2 \times 10^{19}$ W/cm^2. The total duration of the simulations was 15 ps and the targets were either 10 or 20 μm thick. Inter- and intra-species collisions are included in the calculation,[19,20] the effect of which is to slow the hot particles and to heat the initially cold target. It was observed that ≳90% of the hot-electron energy was converted into thermal energy of the target primarily as a result of direct *e*–*e* collisions, with only a few percent being either lost or converted into electromagnetic-field energy.

Figure 109.41 shows the peak temperatures attained by 20-μm-thick targets that have been taken on a slice transverse to the target normal at a depth of 5 μm. In the left (right)-hand column, 10 (30) J of energy was introduced into hot electrons. The target volume was 1.28×10^{-4} (5.12×10^{-4}) mm^3 in the first (second) row. The smallest target reaches a peak temperature of ~500 eV, while the most massive ~100 eV. Only one quadrant of each foil was modeled, the remainder completed by assuming symmetry about the *x* and *y* axes. *LSP* assumes an ideal equation of state (EOS) for the various particle species. Here, the temperatures have been renormalized assuming a Thomas–Fermi EOS.

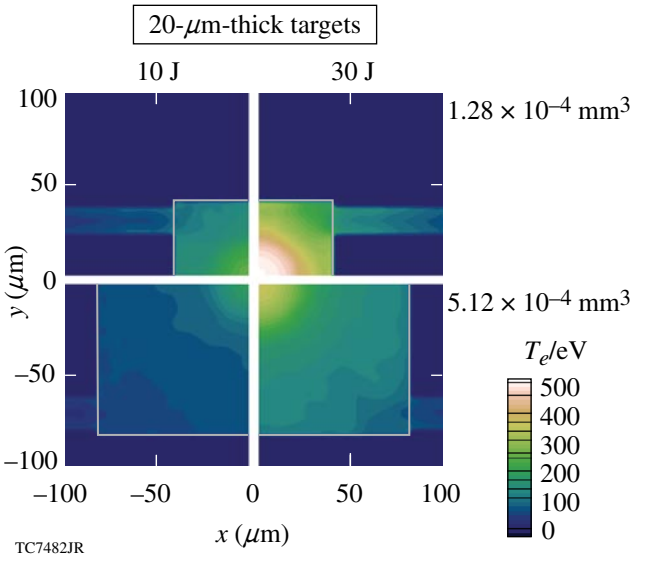

Figure 109.41
The images show target heating from four 3-D *LSP* calculations on a slice perpendicular to the target normal taken at a depth of 5 μm from the target surface. The heating was computed with 10 J and 30 J of energy in hot electrons (columns) and for target volumes of $V = 1.28 \times 10^{-4}$ and 5.12×10^{-4} mm^3 (rows). Only one quadrant of each foil was modeled, the remainder completed by assuming symmetry about the *x* and *y* axes.

1. Reasons for the Absence of Enhanced Stopping in the *LSP* Calculations

The stopping power of hot electrons can be increased above that due to particle collisions by the presence of resistive electric fields.[8,52] The current carried by the hot, laser-produced electrons far exceeds the Alfvén-limiting current for vacuum propagation, $I_A = 17\gamma_b\beta_b$kA,[56] where β_b is the beam velocity normalized to the speed of light, $\beta_b = v_b/c$, and γ_b is the relativistic gamma factor $\gamma_b = (1+\beta_b^2)^{-1/2}$. Estimating the current according to $I \sim \eta_{L\to e}\, eI_L A/T_{\rm hot} = 25$ MA for $I_L = 10^{19}$ W/cm^2, $A = \pi \times (20)^2\ \mu$m^2, $\eta_{L\to e} = 0.2$, and $T_{\rm hot} = 1$ MeV. This is several hundred times larger than the Alfvén limit $I_{\rm hot} \sim 560\left[2.7/(\gamma_b\beta_b)\right]I_A$.

Such beams cannot propagate unless there is a compensating return current. In metals and plasmas, the return current is naturally provided by cold electrons. The cold current represents a drag on the hot component through the resistive electric field $\vec{E} = \vec{j}/\sigma$, where σ is the electrical conductivity (assuming scalar conductivity and neglecting the Hall term). The resistive electric field $E \cong j/\sigma$ may be estimated to be ~2×10^5 kV/cm for the above parameters. This would stop a 1-MeV electron in ~50 μm. In making this estimate, a conductivity of $\sigma = 1 \times 10^6\ \Omega^{-1}$m^{-1} has been assumed. This value is representative of the minimum conductivity of copper (other mid-*Z* metals are similar). Typically this minimum occurs at a few 100 eV, thereafter increasing with temperature $\sigma \sim T_e^{3/2}$ according to the Spitzer value.

Resistive inhibition would be expected to be dominant, if the characteristic range due to the resistive electric field is small compared with the range due to binary collision events s_0. The range estimated above is shorter than the range in copper of $s_0 =$ 700 (3800) μm for 1.0 (5.0)-MeV electrons, respectively. In the current experiments, this is not the full story. In the thin-foil case, $d < s_0$, the "resistive" range should instead be compared with the foil thickness *d*. This is because refluxing hot electrons can contribute significantly to the return current for times greater than a hot-electron transit time. For this reason the *LSP* calculations indicate that resistive inhibition is not an important effect for the parameters of the experiments of Ref. 18. This is further borne out by the predictions of the semi-analytic model that are consistent with the usual stopping power.

Sources of plasma resistivity that are not currently modeled by *LSP*, such as ion-acoustic turbulence, possibly resulting from instability of the return current, have the potential to modify this picture. If the anomalous resistivity were to be a few times larger than the maximum resistivity quoted above, then the resistive range would become smaller than the typical target thickness. This could substantially reduce the contribution of hot electrons to the return current.

2. Effect of Target Heating on K-Shell Line Ratios

The effect of target heating on the relative emission probability of the K_β line has been estimated by adjusting the emission probability p_{K_β} in the *LSP* calculations, according to Fig. 109.40, using the local temperature at the time when the emission process took place. The *LSP* predictions for the line ratio N_{K_β}/N_{K_α}, for three target volumes and 10 (30) J of hot-electron energy, are shown by the light upper (dark lower) open diamonds in Fig. 109.42. Figure 109.42 also shows the experimentally determined ratio of K_β to K_α yield N_{K_β}/N_{K_α} from the RAL 100-TW (crosses) and RAL PW (squares, diamonds, and circles) as a function of target volume.

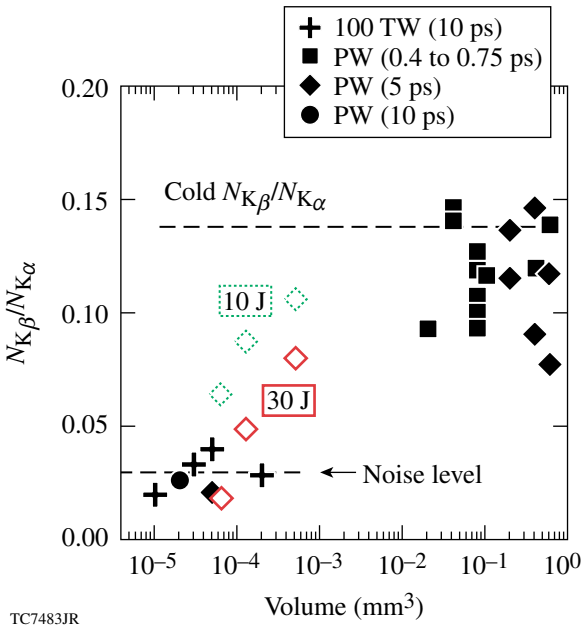

Figure 109.42
Experimental ratio of K_β to K_α yield N_{K_β}/N_{K_α} from the RAL 100-TW (crosses) and RAL PW (squares, diamonds, and circles) as a function of target volume. The open diamonds show *LSP* predictions in the cases of 10 J of energy in hot electrons (upper light) and 30 J (lower dark).

The scatter in the experimental data is too large for the consistency check to be conclusive, especially considering that the experimental K_β signals, for target volumes $V \lesssim 10^{-4}$ mm, are very close to the noise level of the detector at ~3%. It can be said, however, that the PW data are not inconsistent with a hot-electron conversion efficiency of 10%. For example, the close agreement of the 30-J calculations with the experimental data point (shot 5021803) at $V = 5 \times 10^{-5}$ mm^3, where the energy in the central spot was ~150 J.

3. Spatially Resolved K-Shell Emission

The spatial distribution of the K-shell emission reflects the trajectories of the hot electrons[57] and also the volumetric heating profile. Although the K-shell emission was not imaged in Ref. 18, images of the K_α emission from the *LSP* calculation can be produced (Fig. 109.43).

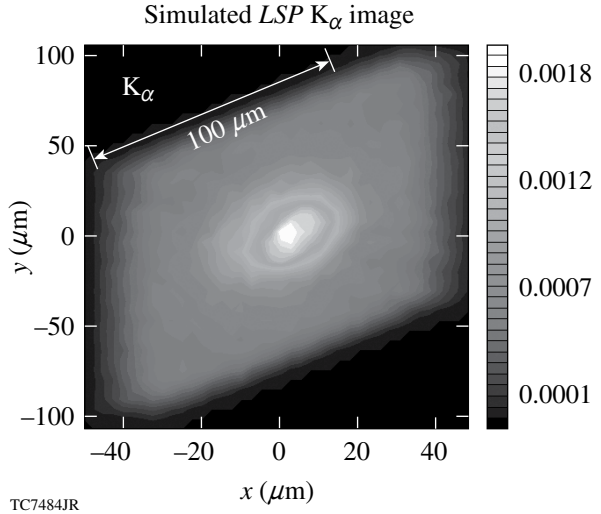

Figure 109.43
Image of K_α emission obtained from 3-D *LSP* calculations.

Conclusions

A semi-analytic model has been developed, and implicit-hybrid particle-in-cell code simulations (*LSP*)[19,20] have been performed to study fast-electron propagation, inner-shell x-ray photon production, and heating of mid-*Z*, mass-limited targets.

For the conditions considered, motivated by RAL experiments,[18] hot-electron flow within the target is dominated by refluxing at the electrostatic sheath at the target surface. This effect is responsible for the observed absolute x-ray yield. The semi-analytic model has been used to demonstrate the insensitivity of the yield to target geometry and hot-electron temperature under the conditions of hot-electron refluxing and classical stopping.

The experimental K_α yields are consistent between both models and experiment for an intensity-independent electron

conversion efficiency of ~10%. This result raises some concerns since 15% to 50% conversion efficiencies have been reported in the literature, e.g., Refs. 1, 6, 7, and 15. Surface fields[18] or anomalous stopping mechanisms, e.g., Ref. 58, might prevent hot electrons from penetrating to the cold interior of the target where they can efficiently produce K_α photons. If this were the case, a higher hot-electron conversion efficiency would be required to produce the observed K_α yields.[18] Target expansion is not a likely explanation for the discrepancy because it is responsible for only a few-percent decrease in the target density over the period of K_α emission. The ratio of K_β to K_α line emission is related to the degree of target heating that may be used as a consistency check on the hot-electron conversion efficiency.

Three-dimensional *LSP* calculations of volumetric target heating have been performed giving predictions for line ratios as a function of hot-electron conversion efficiency. At present, the experimental data set is not sufficiently precise to conclusively choose between the predictions; however, it does suggest the usefulness of the technique, which will be pursued in future experiments on OMEGA EP.

ACKNOWLEDGMENT

This work was supported by the U.S. Department of Energy Office of Inertial Confinement Fusion under Cooperative Agreement No. DE-FC52-92SF19460, the University of Rochester, and the New York State Energy Research and Development Authority. The support of DOE does not constitute an endorsement by DOE of the views expressed in this article.

REFERENCES

1. M. H. Key, M. D. Cable, T. E. Cowan, K. G. Estabrook, B. A. Hammel, S. P. Hatchett, E. A. Henry, D. E. Hinkel, J. D. Kilkenny, J. A. Koch, W. L. Kruer, A. B. Langdon, B. F. Lasinski, R. W. Lee, B. J. MacGowan, A. MacKinnon, J. D. Moody, M. J. Moran, A. A. Offenberger, D. M. Pennington, M. D. Perry, T. J. Phillips, T. C. Sangster, M. S. Singh, M. A. Stoyer, M. Tabak, G. L. Tietbohl, M. Tsukamoto, K. Wharton, and S. C. Wilks, Phys. Plasmas **5**, 1966 (1998).
2. P. A. Norreys *et al*., Phys. Plasmas **6**, 2150 (1999).
3. K. A. Tanaka *et al*., Phys. Plasmas **7**, 2014 (2000).
4. J. A. Koch *et al*., Phys. Rev. E **65**, 016410 (2001).
5. R. B. Stephens *et al*., Phys. Rev. E **69**, 066414 (2004).
6. S. C. Wilks *et al*., Phys. Rev. Lett. **69**, 1383 (1992).
7. B. F. Lasinski *et al*., Phys. Plasmas **6**, 2041 (1999).
8. L. Gremillet *et al*., Phys. Plasmas **9**, 941 (2002).
9. Y. Sentoku *et al*., Phys. Rev. Lett. **90**, 155001 (2003).
10. M. Tabak *et al*., Phys. Plasmas **1**, 1626 (1994).
11. N. G. Basov, S. Yu. Gus'kov, and L. P. Feokistov, J. Sov. Laser Res. **13**, 396 (1992).
12. O. L. Landen *et al*., Rev. Sci. Instrum. **72**, 627 (2001).
13. H.-S. Park *et al*., Rev. Sci. Instrum. **75**, 4048 (2004).
14. K. Yasuike *et al*., Rev. Sci. Instrum. **72**, 1236 (2001).
15. K. B. Wharton *et al*., Phys. Rev. Lett. **81**, 822 (1998).
16. R. Kodama *et al*., Phys. Plasmas **8**, 2268 (2001).
17. J. D. Hares *et al*., Phys. Rev. Lett. **42**, 1216 (1979).
18. W. Theobald, K. Akli, R. Clarke, J. Delettrez, R. R. Freeman, S. Glenzer, J. Green, G. Gregori, R. Heathcote, N. Izumi, J. A. King, J. A. Koch, J. Kuba, K. Lancaster, A. J. MacKinnon, M. Key, C. Mileham, J. Myatt, D. Neely, P. A. Norreys, H.-S. Park, J. Pasley, P. Patel, S. P. Regan, H. Sawada, R. Shepherd, R. Snavely, R. B. Stephens, C. Stoeckl, M. Storm, B. Zhang, and T. C. Sangster, Phys. Plasmas **13**, 043102 (2006).
19. D. R. Welch *et al*., Nucl. Instrum. Methods Phys. Res. A **464**, 134 (2001).
20. D. R. Welch *et al*., Phys. Plasmas **13**, 063105 (2006).
21. G. Gregori *et al*., Contrib. Plasma Phys. **45**, 284 (2005).
22. F. Pisani *et al*., Phys. Rev. E **62**, R5927 (2000).
23. E. Martinolli *et al*., Phys. Rev. E **73**, 046402 (2006).
24. H. Chen, B. Soom, B. Yaakobi, S. Uchida, and D. D. Meyerhofer, Phys. Rev. Lett. **70**, 3431 (1993).
25. A. Rousse *et al*., Phys. Rev. E **50**, 2200 (1994).
26. D. C. Eder *et al*., Appl. Phys. B **70**, 211 (2000).
27. R. P. J. Town *et al*., Nucl. Instrum. Methods Phys. Res. A **544**, 61 (2005).
28. A. J. Mackinnion *et al*., Phys. Rev. Lett. **88**, 215006 (2002).
29. H. Chen and S. C. Wilks, Laser Part. Beams **23**, 411 (2005).
30. S. P. Hatchett, C. G. Brown, T. E. Cowan, E. A. Henry, J. S. Johnson, M. H. Key, J. A. Koch, A. B. Langdon, B. F. Lasinski, R. W. Lee, A. J. MacKinnon, D. M. Pennington, M. D. Perry, T. W. Phillips, M. Roth, T. C. Sangster, M. S. Singh, R. A. Snavely, M. A. Stoyer, S. C. Wilks, and K. Yasuike, Phys. Plasmas **7**, 2076 (2000).
31. R. A. Snavely, M. H. Key, S. P. Hatchett, T. E. Cowan, M. Roth, T. W. Phillips, M. A. Stoyer, E. A. Henry, T. C. Sangster, M. S. Singh, S. C. Wilks, A. MacKinnon, A. Offenberger, D. M. Pennington, K. Yasuike, A. B. Langdon, B. F. Lasinski, J. Johnson, M. D. Perry, and E. M. Campbell, Phys. Rev. Lett. **85**, 2945 (2000).
32. U. Teubner, I. Uschmann, P. Gibbon, D. Altenbernd, E. Föster, T. Feurer, W. Theobald, R. Sauerbrey, G. Hirst, M. H. Key, J. Lister, and D. Neely, Phys. Rev. E **54**, 4167 (1996).
33. D. Salzmann *et al*., Phys. Rev. E **65**, 036402 (2002).

34. F. Ewald, H. Schwoerer, and R. Sauerbrey, Europhys. Lett. **60**, 710 (2002).

35. Ch. Reich *et al*., Phys. Rev. Lett. **84**, 4846 (2000).

36. H. Kolbenstvedt, J. Appl. Phys. **38**, 4785 (1967).

37. M. Green, Solid-State Electron. **3**, 314 (1961).

38. C. Stoeckl, J. A. Delettrez, J. H. Kelly, T. J. Kessler, B. E. Kruschwitz, S. J. Loucks, R. L. McCrory, D. D. Meyerhofer, D. N. Maywar, S. F. B. Morse, J. Myatt, A. L. Rigatti, L. J. Waxer, J. D. Zuegel, and R. B. Stephens, Fusion Sci. Technol. **49**, 367 (2006).

39. M. Green and V. E. Cosslett, J. Phys. D **1**, 425 (1968).

40. T. Feurer, W. Theobald, R. Sauerbrey, I. Uschmann, D. Altenbernd, U. Teubner, P. Gibbon, E. Förster, G. Malka, and J. L. Miquel, Phys. Rev. E **56**, 4608 (1997).

41. W. Bambynek *et al*., Rev. Mod. Phys. **44**, 716 (1972).

42. S. M. Seltzer, in *Monte Carlo Transport of Electrons and Photons*, edited by T. M. Jenkins, W. R. Nelson, and A. Rindi (Plenum Press, New York, 1988), Chap. 7, pp. 153–181.

43. Assuming that the hot-electron density within the foil is uniform, we can estimate the absorption fraction by $f_{\text{abs}} = (L_a/d)\left[1 - \exp\left(-d/L_a\right)\right]$ with the linear attenuation length $L_a = 22.3$ μm for K_α photons.

44. M. I. K. Santala *et al*., Phys. Rev. Lett. **84**, 1459 (2000).

45. G. Malka and J. L. Miquel, Phys. Rev. Lett. **77**, 75 (1996).

46. D. W. Forslund, J. M. Kindel, and K. Lee, Phys. Rev. Lett. **39**, 284 (1977).

47. F. N. Beg *et al*., Phys. Plasmas **4**, 447 (1997).

48. F. Juettner, Ann. Phys. **34**, 856 (1911).

49. M. J. Berger, in *Methods in Computational Physics: Advances in Research and Applications*, edited by B. Alder, S. Fernbach, and M. Rotenberg, Volume 1: Statistical Physics (Academic Press, New York, 1963), pp. 135–215.

50. The total K-shell ionization cross section is from Ref. 36, and, unlike the cross section in Refs. 37 and 39, it is good for relativistic electron energies.

51. C. Hombourger, J. Phys. B, At. Mol. Opt. Phys. **31**, 3693 (1998).

52. A. R. Bell *et al*., Plasma Phys. Control. Fusion **39**, 653 (1997).

53. R. J. Mason, E. S. Dodd, and B. J. Albright, Phys. Rev. E **72**, 015401(R) (2005).

54. R. M. More, Adv. At. Mol. Phys. **21**, 305 (1985).

55. P. K. Patel, M. H. Key, A. J. Mackinnon, R. Berry, M. Borghesi, D. M. Chambers, H. Chen, R. Clarke, C. Damian, R. Eagleton, R. Freeman, S. Glenzer, G. Gregori, R. Heathcote, D. Hey, N. Izumi, S. Kar, J. King, A. Nikroo, A. Niles, H.-S. Park, J. Pasley, N. Patel, R. Shepherd, R. A. Snavely, D. Steinman, C. Stoeckl, M. Storm, W. Theobald, R. Town, R. Van Maren, S. C. Wilks, and B. Zhang, Plasma Phys. Control. Fusion **47**, B833 (2005).

56. H. Alfvén, Phys. Rev. A **55**, 425 (1939).

57. Ch. Reich *et al*., Phys. Rev. E **68**, 056408 (2003).

58. M. Honda, J. Meyer-ter-Vehn, and A. Pukhov, Phys. Rev. Lett. **85**, 2128 (2000).